ResearchGate

See discussions, stats, and author profiles for this publication at: https://www.researchgate.net/publication/279564481

Automatic detection of region-mura defect in TFT-LCD

Article *in* IEICE Transactions on Information and Systems · October 2004

Source: search.ieice.org

CITATIONS
77

READS
442

2 authors, including:

Suk I. Yoo

76 PUBLICATIONS **567** CITATIONS

SEE PROFILE

All content following this page was uploaded by Suk I. Yoo on 23 December 2013.

The user has requested enhancement of the downloaded file.

PAPER

Automatic Detection of Region-Mura Defect in TFT-LCD

Jae Y. LEE[†a)] ***and*** **Suk I. YOO**[†b)]**,** ***Nonmembers***

SUMMARY Visual defects, called mura in the field, sometimes occur during the manufacturing of the flat panel liquid crystal displays. In this paper we propose an automatic inspection method that reliably detects and quantifies TFT-LCD region-mura defects. The method consists of two phases. In the first phase we segment candidate region-muras from TFT-LCD panel images using the modified regression diagnostics and Niblack's thresholding. In the second phase, based on the human eye's sensitivity to mura, we quantify mura level for each candidate, which is used to identify real muras by grading them as pass or fail. Performance of the proposed method is evaluated on real TFT-LCD panel samples.

key words: *Machine vision, image segmentation, regression diagnostics, industrial inspection, visual perception.*

1. Introduction

Recently, TFT-LCD (Thin Film Transistor Liquid Crystal Display) devices have become a major technology for FPD (Flat Panel Display). As the FPD market becomes more and more competitive, the quality of the display becomes a more critical issue for manufacturers. The most important process to control the quality of the display is to inspect visual defects that sometimes occur during the manufacturing of the flat panel liquid crystal displays. Human visual inspection, which is still used by most manufacturers, has a number of drawbacks including limitations of human sensitivity, inconsistent detection due to human subjectivity, and high cost. Automatic inspection using machine vision techniques can overcome many of these disadvantages and offer manufacturers an opportunity to significantly improve quality and reduce costs.

One class of defects includes a variety of blemishes, called *mura** in the field, which appear as low contrast and non-uniform brightness regions, typically larger than single pixels [12], [15]. They are caused by a variety of physical factors such as non-uniformly distributed liquid crystal material and foreign particles within the liquid crystal. Depending on the shapes and sizes, mura defects may be classified into spot-mura, line-mura, and region-mura defect. Figure 1 contains sketch of several mura defects. Compared to spot-mura and line-mura, region-mura is relatively difficult to be identified due to its low contrast and irregular pattern of shape. In this paper, we thus present the technique focused on region-mura.

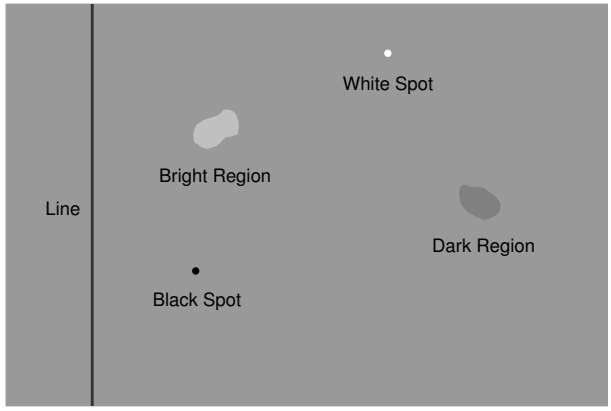

Fig. 1 Example of line-mura, spot-mura, and region-mura defects.

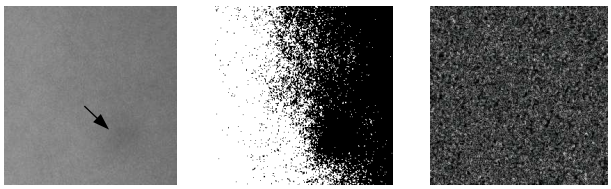

Fig. 2 (a) Sample subimage of a TFT-LCD image having a dark region-mura, which position is indicated by an arrow. (b) Thresholding result of (a) using Otsu's method. (c) Gradient magnitude image of (a).

The problem of segmenting region-muras reliably from TFT-LCD images is not easy with conventional methods. Although it is not significant, TFT-LCDs generally have the intrinsic non-uniformity due to the variance of the backlight and uneven distributions of liquid crystal material. This overall non-uniformity and the low contrast of the region-mura make it hard to apply simple thresholding directly. Otsu's method [5], for example, cannot solve the problem properly as il-

Manuscript received January 1, 2004.
Manuscript revised January 1, 2004.
Final manuscript received January 1, 2004.

[†]The authors are with the School of Computer Science and Engineering, Seoul National University, Shilim-Dong, Gwanak-Gu, Seoul 151-742, Korea.
a) E-mail: leejy@ailab.snu.ac.kr
b) E-mail: siyoo@ailab.snu.ac.kr

*Mura is a Japanese word meaning blemish that has been adopted in English to provide a name for imperfections of a display pixel matrix surface that are visible when the display screen is driven to a constant gray level.

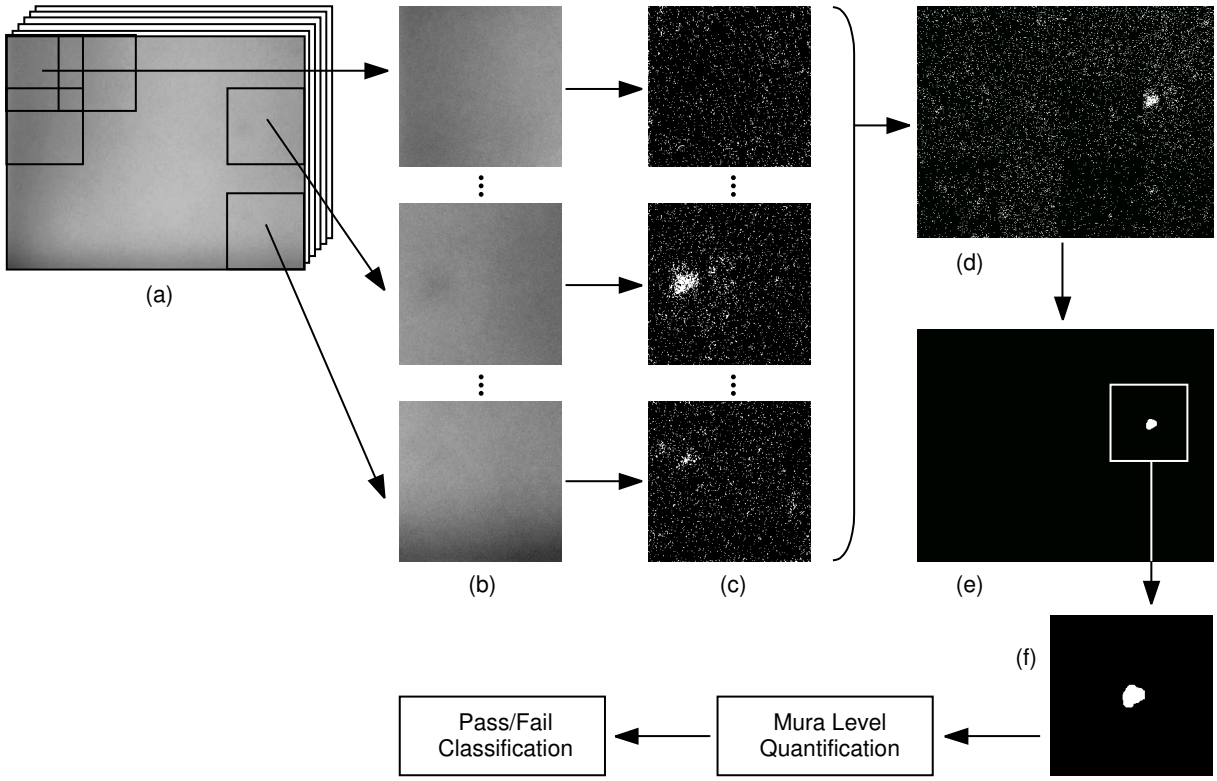

Fig. 3 Overview of our region-mura inspection procedure. (a) Input image. (b) Extracted windows ($W \times H$ pixels). (c) Local segmentation results. (d) Merged segmentation result. (e) Post-processed image. (f) Extracted candidate region-mura which mura level is to be quantified.

lustrated in Fig. 2(b). Also, region-muras have smooth change of brightness from their surrounding regions, and therefore, they have no clear edge as shown in Fig. 2(c). This characteristic invalidates the preconditions required for gradient magnitude based approaches [9], [13]. Another problem in TFT-LCD image quality inspection is to quantify mura level for each region-mura. Quantification is necessary to control a mura acceptance level according to the panel quality level required by the industry.

In this paper we describe an automatic inspection method that reliably detects and quantifies TFT-LCD region-mura defects. The method consists of two phases. In the first phase we segment candidate region-muras from TFT-LCD panel images using the modified regression diagnostics [6] and Niblack's thresholding [7]. In the second phase, based on the human eye's sensitivity to mura, we quantify mura level for each candidate, which is used to identify real muras by grading them as pass or fail.

2. Approach Overview

The overall inspection procedure is shown in Fig. 3. For each TFT-LCD panel under test, predefined full-screen constant test patterns are displayed to produce digital input images. Figure 3(a) shows a TFT-LCD panel image captured when the display screen is driven to a constant gray pattern. Each input image is then divided into overlapping windows for local processing. The window size, $W \times H$, and the amount of overlapping, ΔW and ΔH, are estimated from a *priori* knowledge. Segmentation of region-mura is performed on each window and the local segmentation results are merged into a single binary image with their original positions in the input image, as shown in Fig. 3(d). This local processing is to reduce the overall non-uniformity in the input image. The merged binary image is then post-processed by median filtering, morphological closing, and morphological opening [16] to remove noise and refine the segmentation result. Finally candidate region-muras are extracted from the post-processed image and their mura levels are quantified in order to identify real muras.

The most critical part of our approach is to segment region-muras from each window image, which can be outlined as follows:

1. We use the modified regression diagnostics to roughly estimate the background region in the window image. The estimated background region is then approximated by a low order polynomial to generate a background surface.
2. Subtraction of the background surface from the

original window image is used to find threshold to obtain the binary segmentation result. This subtraction is to remove the influence of non-uniform background and transform the segmentation problem into a simple thresholding one.

Section 3 describes our local segmentation procedure in detail. Section 4 presents human perception model and quantification formula on mura level. In Sect. 5, performance of our method is evaluated on real TFT-LCD panel samples, and finally the conclusion is presented in Sect. 6.

3. Local Segmentation

3.1 Background Surface Estimation

To remove the influence of non-uniform background, we first have to estimate background surface robustly. The problem of background surface estimation can be viewed as a robust regression problem in data fitting [8]. Let I be a window image of size $W \times H$ pixels. Each pixel located at (x, y) with the intensity value z_{xy}, called a *data pixel*, will be denoted by $(x, y; z_{xy})$ for $x = 1, \ldots, W$, $y = 1, \ldots, H$. The *data set* is then defined to be a set of data pixels as

$$\Psi = \{(x, y; z_{xy}) | x = 1, \ldots, W, y = 1, \ldots, H\}. \quad (1)$$

The data set is approximated by a bivariate polynomial model $f^{(d)}(x, y)$ of order d,

$$f^{(d)}(x, y) = \sum_{m+n \le d} a_{mn} x^m y^n, \quad (2)$$

such that $f^{(d)}(x, y)$ gives the estimated intensity value at (x, y) for $x = 1, \ldots, W$, $y = 1, \ldots, H$. The residual of the xyth data pixel with respect to $f^{(d)}$, denoted by r_{xy}, is the difference between the original and the estimated intensity of the xyth data pixel given by

$$r_{xy} = z_{xy} - f^{(d)}(x, y). \quad (3)$$

The simplest way to estimate the model parameters, a_{mn}'s, may be the least-squares (LS) regression method, in which the model parameters are estimated by minimizing the sum of the squared residuals:

$$\min \sum_{x,y} r_{xy}^2. \quad (4)$$

The LS method, however, performs poorly in terms of robustness because even a single aberrant data point, or an outlier, can completely perturb the regression result [8].

In our approach, we use a modified version of regression diagnostics [6] to estimate the background surface robustly. Diagnostics are certain quantities computed from the data with the purpose of pinpointing aberrant data points, after which these outliers can be removed, followed by a LS analysis on the remaining ones. Our background surface estimation algorithm, when the size of region-mura is upper-bounded by $\alpha\%$ of the window size, works as follows:

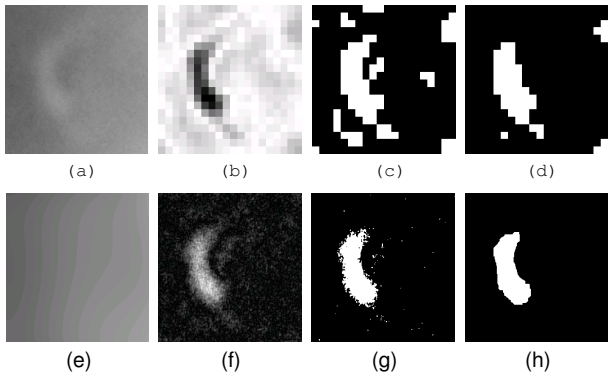

Fig. 4 The process of local segmentation ($l = 2, h = 4$). (a) Input window image. (b) Computed diagnostic measure J. (c) Constructed binary image with $\alpha = 20$. (d) Median-filtered image of (c). (e) Estimated background surface $f_B^{(h)}$. (f) Absolute residuals with respect to $f_B^{(h)}$. (g) Thresholding result of residuals with $T = 2$. (h) Post-processing result.

1. For each data pixel p in Ψ,
   a. Remove p from the data set. Let Ψ_{-p} be the resulting data set:
   $$\Psi_{-p} = \Psi - \{p\}. \quad (5)$$
   b. Determine the polynomial of order l fitting Ψ_{-p}, denoted by $f_{-p}^{(l)}$, using the LS.
   c. Compute the diagnostic measure $J(p)$ defined to be the mean of the absolute residuals of the data pixels in Ψ_{-p} with respect to $f_{-p}^{(l)}$:
   $$J(p) = \frac{1}{WH - 1} \sum_{\Psi_{-p}} |z_{xy} - f_{-p}^{(l)}(x, y)|. \quad (6)$$
2. Construct a binary image so that $\alpha\%$ data pixels which have small value of J are classified as white with value one and the others as black with value zero.
3. Apply median filtering to the binary image.
4. Remove probable outliers from Ψ by excluding data pixels which correspond to the white pixels in the median-filtered binary image, giving an estimation of the background region denoted by Ψ_B.
5. Determine the polynomial of order h fitting Ψ_B, denoted by $f_B^{(h)}$, using the LS.

The order of polynomial for diagnostics measure, l, is determined to be the average order of the background variations of the LCD panel images and the order for final background fitting, h, is determined to be the maximal order of the background variations, where the order of background variation is defined to be the least order of polynomial that can fit the background with

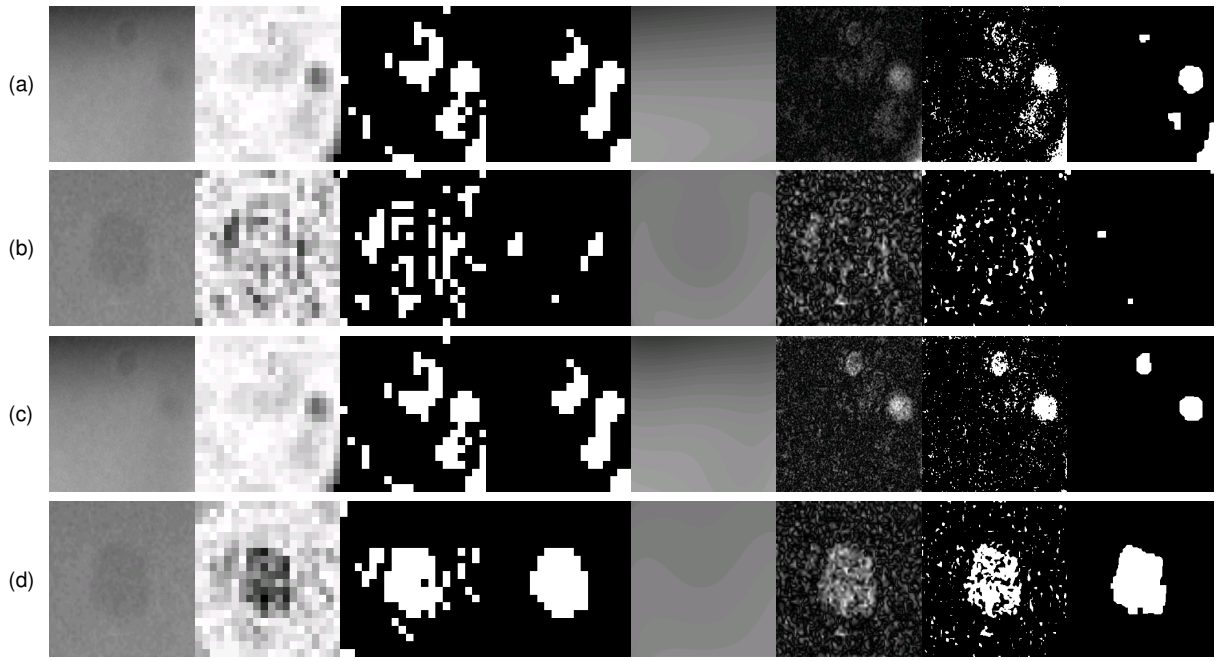

Fig. 5 Single polynomial model versus composite model: (a) biquadratic ($d = 2$) for both diagnostics measure and background fitting; (b) biquartic ($d = 4$) for both diagnostics measure and background fitting; (c)–(d) biquadratic for diagnostics measure and biquartic for background fitting. The input image of (c) is same as (a) and the input image of (d) is same as (b). From left to right, each column corresponds to input window image, diagnostics measure, constructed binary image, median-filtered binary image, background surface fit, absolute residuals, thresholding result of residuals ($T = 2$), and post-processing result.

acceptable fitting error less than predefined threshold.

The process of background surface estimation is illustrated in Fig. 4. When the size of a region-mura is much less than $\alpha WH/100$ pixels or the window image has no region-mura, however, some background pixels may be included in the $\alpha\%$ data pixels. The median filtering solves this problem to some extent as shown in Fig. 4(d). It should be pointed out that a fixed thresholding on J is not probable since the range of J varies widely over images according to the contrast and size of the region-muras and the degree of non-uniformity of the background. The estimated background surface reflects the brightness variations of the background quite well as shown in Fig. 4(e).

We use two polynomial models of different orders for the background surface estimation: one of order l for diagnostics measure and the other of order h for final background fitting. The LCD panel images have varying order of background non-uniformity over images. Therefore, with a fixed single polynomial model, it is hard to fit them effectively: If the order of polynomial model is less than the variations in the background, some background pixels, which are not fitted by the model, can be incorrectly classified as outliers (Fig. 5(a)). Moreover some weak region-muras can be missed due to incorrect fitting. On the other hand, if the order of polynomial model is too high, it can overfit the data set including outliers and give unreliable diagnostic measures especially when the size of the region-mura is large (Fig. 5(b)). In our two-model strategy, the overfit is minimized using the low order polynomial model and the possible misclassifications are corrected by the high order model (Fig. 5(c) and (d)).

3.2 Thresholding

Previously, we have robustly estimated the background surface $f_B^{(h)}$ including the background region Ψ_B. Let r^*_{xy} be the residual of the xyth data pixel with respect to $f_B^{(h)}$ given by

$$r^*_{xy} = z_{xy} - f_B^{(h)}(x, y). \tag{7}$$

The segmentation problem is then transformed into a simple thresholding one on the residuals. The threshold is determined based on the distribution of the residuals of the background pixels. Let μ be the residual mean and σ be the standard deviation of the residuals of the background pixels given by

$$\mu = \frac{1}{|\Psi_B|} \sum_{(x,y;z_{xy})\in\Psi_B} r^*_{xy} \tag{8}$$

$$\sigma^2 = \frac{1}{|\Psi_B|} \sum_{(x,y;z_{xy})\in\Psi_B} (r^*_{xy} - \mu)^2, \tag{9}$$

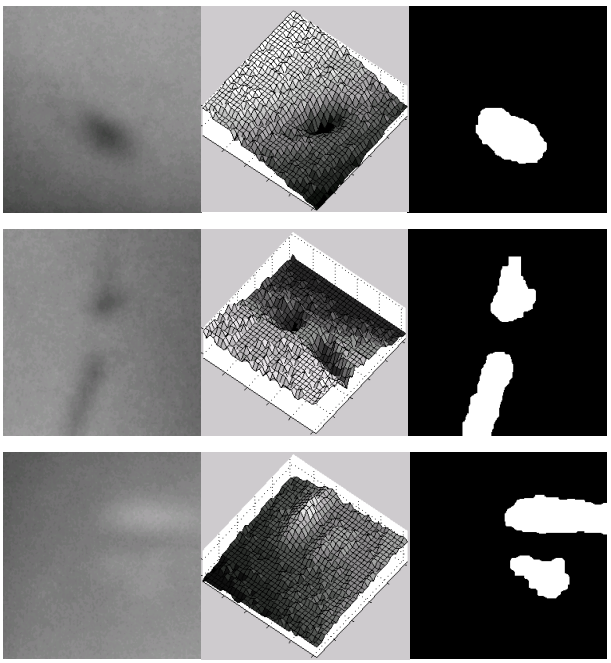

Fig. 6 Segmentation examples.

where $|\Psi_B|$ is the cardinality of Ψ_B. For a given threshold T, according to Niblack's method [7], the image is then segmented into a binary image so that the defect region is to be white with value one and the background region to be black with value zero as follows:

$$Z(x,y) = \begin{cases} 1, & |r^*_{xy} - \mu|/\sigma > T \\ 0, & |r^*_{xy} - \mu|/\sigma \leq T \end{cases} \tag{10}$$

Resulting binary images are merged into a single binary image as described in Sect. 2 and then post-processed, giving candidate region-muras. Figure 6 shows three examples with their original window images, 3D views, and final images processed. In Fig. 6, the top image has one dark circular mura, the middle image has two dark muras, and the bottom image has two adjacent bright muras, and all muras were successfully segmented.

4. Visual Perception Based Identification

In order to identify the real region-muras from the candidates found in the previous section, the properties of the human visual perception have to be considered. In this section, we first present human perception model and, based on it, formulate a measurement index on mura level. The final identification procedure is then followed.

4.1 Visual Perception Model

The fovea is always focused on the object of interest by the accommodation ability of the eye. The typical simulation of the retina consists of object region, object-background region, and surround-background region

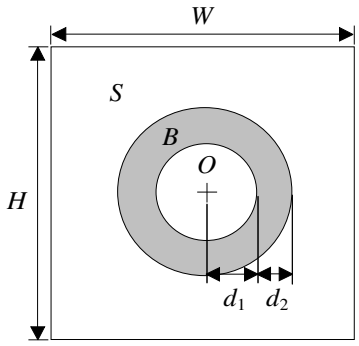

Fig. 7 Observation field for computation of mura level.

with different luminance stimuli [14]. The regions are arranged in the observation field as concentric ones, with the object in the middle followed by the object-background and the surround-background as shown in Fig. 7. The object-background is the close neighborhood of the object that has a strong influence on the perception of the object. The width of the object-background is set to be a half of radiate distance from the object center such that $d_2 = 0.5d_1$. Its size is biologically motivated [10]. The surround-background region consists of the area of the complete retina and has a relatively weak influence on the perception of the object. The luminance stimulus of each region can be simplified to the mean of the gray intensity of the corresponding region in the image and will be denoted by I_o for the object, I_b for the object-background, and I_s for the surround-background, respectively. If the surround-background is uniform and $I_s = I_b$, we can ignore its influence on the perception of the object [2].

4.2 Measurement Index on Mura Level

The ability of the eye to discriminate between changes in luminance is explained by Weber's law [1]: if L and $L + \Delta L$ are just noticeably different luminances, $\Delta L/L$ is nearly a constant C_w (C_w is Weber's constant). According to Weber's law, in the luminance term, the level of visibility of an object can be expressed as

$$Q_L = \frac{|L_o - L_b|/L_b}{C_w}, \tag{11}$$

where L_o denotes luminance stimuli of the object and L_b denotes luminance stimuli of the object-background. The luminance stimuli of the surround-background L_s is ignored in Eq. (11), assuming uniform surround such that $L_s = L_b$. In the image intensity term, we can discard the influence of L_b on ΔL from Eq. (11) since the luminance is unevenly mapped to gray level in FPD devices so that ΔI's, the just-noticeable intensity difference, are nearly equal over all gray levels (e.g., 256 gray levels for 8-bit display) when the object size is fixed. Under this consideration Eq. (11) can be transformed into

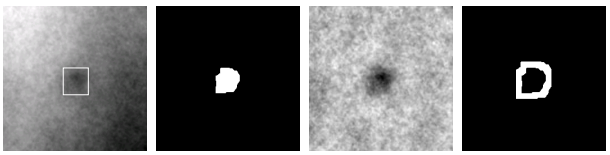

Fig. 8 (a) A window image with a candidate region-mura in the middle. The minimal bounding rectangle is displayed with white color. (b) The region of the candidate region-mura. (c) The intensity-scaled residual image to have maximum 255 and minimum 0. (d) The region of the object-background.

$$Q_I = \frac{|I_o - I_b|}{\Delta I}. \tag{12}$$

The just-noticeable intensity difference (JND), ΔI, increases quickly as the object area decreases [3]. In a recent SEMI standard on FPD [17], using ergonomics approach, the relation between mura area and JND has been formulated as

$$JND = 1.97/A^{0.33} + 0.72, \tag{13}$$

where A is the area of a mura. Finally, from Eq. (12) and Eq. (13), we thus have the following measurement index on mura level:

$$Q_I = \frac{|I_o - I_b|}{1.97/A^{0.33} + 0.72}. \tag{14}$$

4.3 Identification

For each candidate region-mura, we first locate a $W \times H$ window such that the minimal bounding rectangle of the candidate is centered within the window. Let I' be the located window image. Next, by approximating the image surface of I' except the pixels belonging to some candidate region-muras detected, we generate a polynomial surface, $f_B^{(h)}$, of order h. The image I' is then subtracted from $f_B^{(h)}$, giving a residual image R. This subtraction, making $I_s = I_b$, removes the influence of non-uniform surround-background on the perception of the candidate region-mura. The object-background region is obtained by dilating the candidate mura region with $w'/2 \times h'/2$ structuring element [16] and then by excluding the candidate mura region from the dilation result, where w' is the width of the minimal bounding rectangle and h' is the height of the rectangle. Finally, we compute the level of the candidate region-mura from Eq. (14) using I_o, I_b, and A given by

$$I_o = \frac{1}{|\Psi_o|} \sum_{p \in \Psi_o} R(p), \tag{15}$$

$$I_b = \frac{1}{|\Psi_b|} \sum_{p \in \Psi_b} R(p), \text{ and} \tag{16}$$

$$A = |\Psi_o|, \tag{17}$$

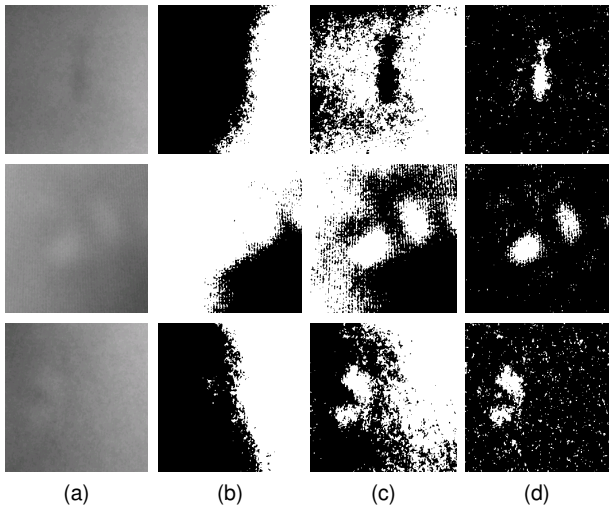

Fig. 9 Experimental results for three sample TFT-LCD panel images. (a) Input images. (b) Results from Otsu's method. (c) Results from Chow and Kaneko's method. (d) Results from our method.

where $R(p)$ is the residual of the data pixel p with respect to $f_B^{(h)}$, Ψ_o is the set of data pixels of the candidate mura region, and Ψ_b is the set of data pixels of the object-background region. If the level of a candidate region-mura exceeds the mura acceptance level required by the industry, the candidate region-mura is identified to be the real. Figure 8 shows an example illustrating this identification procedure.

5. Experiments

5.1 Experiment I

In the first experiment, we compare the segmentation performance of our method with Chow and Kaneko's adaptive thresholding method [4]. Chow and Kaneko employed 256×256 pixel images and divided them into 7×7 blocks of 64×64 pixel subimages with a 50% overlap. For each subimage having bimodal histogram, a threshold was assigned to the center of it. Then the threshold surface was interpolated from these local thresholds, giving every pixel in the image its own threshold. This method historically forms the foundation of local thresholding method, and is frequently cited in the literature.

Figure 9 shows the experimental result for three sample TFT-LCD panel images. The size of each input image in Fig. 9(a) is 256×256 pixels. The global thresholding results from Otsu's method [5] are included to show the underlying non-uniformity in the image backgrounds (Fig. 9(b)). Figure 9(c) shows the segmentation results from Chow and Kaneko's method. The parameters for bimodality test [11] were optimized for each input image. Figure 9(d) is the results from our method with $\alpha = 20$ and $T = 2$.

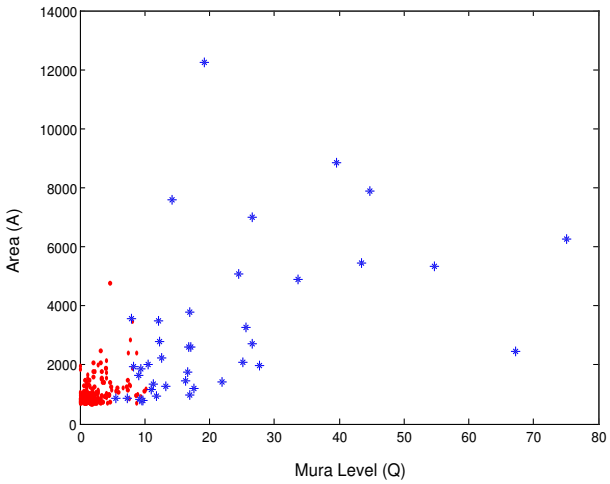

Fig. 10 Plot of mura level and area of all candidate region-muras detected. Candidates claimed by human inspection are denoted by blue asterisk (∗) and the other candidates by red dot (•).

As shown in Fig. 9(c), with Chow and Kaneko's method, the mura regions are localized quite well as like with our method, but some background regions are incorrectly segmented as candidate regions. It is because the bimodality rarely occurs in the background regions and thus interpolation from neighboring thresholds can be ineffective.

5.2 Experiment II

The next experiment has been performed on 200 TFT-LCD panel samples consisting of 30 *bad* panels and 170 *good* panels. Each bad panel has at least one region-mura, totally 40 region-mura defects, which was detected by human visual inspection in the field. Good panels are those claimed to have no defect. The test patterns were black, blue, gray, green, red, and white, and thus 1,200 input images were captured. The resolution of each image is 1280×1024. Each of 1,200 panel images was processed using our inspection algorithm with 256×256 window size and with $l = 2$, $h = 4$, $\alpha = 20$, and $T = 2$, and total 257 candidate have been detected in the first phase when all the identical detections on the same region of a TFT-LCD panel were counted as one. There can be maximum of six detections on the same region of a panel as six different pattern images are captured for each panel. In the second phase, the mura level values of all candidate region-muras were computed. For multiple detection case, the largest mura level value was selected. The mura level value of each real region-mura claimed by human inspection was then greater than 5.5, which is shown with blue asterisk (∗) in Fig. 10, while the average of the mura level values of all the other candidates was less than 5.5, shown with the red dot (•) in Fig. 10. Based on this result, the mura level threshold was set to be 5.5. Figure 11 shows the inspection result for each candidate region-mura and selected candidate images ordered by computed mura level value to demonstrate the correspondence to human visibility. It took 0.49 second, in average, to process each panel image.

#	Q_l	Result	#	Q_l	Result
1	75.17	defect	41	8.93	defect
2	67.28	defect	42	8.78	defect
3	54.62	defect	43	8.76	defect
4	44.67	defect	44	8.63	defect
5	43.52	defect	45	8.22	defect
6	39.6	defect	46	8.11	defect
7	33.73	defect	47	8.08	defect
8	27.69	defect	48	8.02	defect
9	26.65	defect	49	7.85	defect
10	26.54	defect	50	7.78	defect
11	25.66	defect	51	7.66	defect
12	25.16	defect	52	7.65	defect
13	24.47	defect	53	7.46	defect
14	21.94	defect	54	7.31	defect
15	19.16	defect	55	7.25	defect
16	17.61	defect	56	7.23	defect
17	17.07	defect	57	7.14	defect
18	16.96	defect	58	6.63	defect
19	16.92	defect	59	5.93	defect
20	16.83	defect	60	5.72	defect
21	16.64	defect	61	5.63	defect
22	16.37	defect	62	5.56	defect
23	14.27	defect	63	5.56	defect
24	13.19	defect	64	4.85	pass
25	12.56	defect	65	4.69	pass
26	12.25	defect	66	4.62	pass
27	12.2	defect	67	4.61	pass
28	11.81	defect	68	4.52	pass
29	11.31	defect	⋮		
30	10.94	defect			
31	10.51	defect	248	0.06	pass
32	10.21	defect	249	0.06	pass
33	9.93	defect	250	0.06	pass
34	9.76	defect	251	0.04	pass
35	9.59	defect	252	0.03	pass
36	9.55	defect	253	0.03	pass
37	9.42	defect	254	0.03	pass
38	9.35	defect	255	0.01	pass
39	9.27	defect	256	0.01	pass
40	9.02	defect	257	0.01	pass

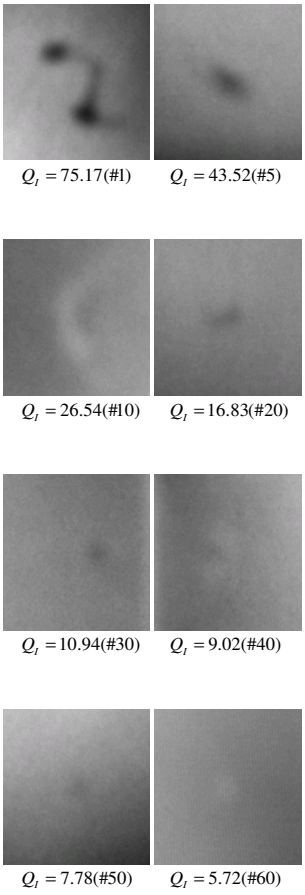

Fig. 11 Inspection results and quantification examples. Real region-muras claimed by human inspection are numbered with italic font.

From this experiment, all 40 region-muras claimed by human inspection have been successfully detected but 23 additional candidates, which are shown in Fig. 12, have been also identified to be real when the mura level threshold was set to be 5.5. These 23 additional defects identified to be real but not claimed by human inspection reflects the limitations of human visual inspection including inconsistency and weak sensitivity. Finally, the mura level threshold can be adjusted according to the panel quality level required by the industry: the threshold can be lowered until all weak defects required by industry can be detected or made larger to detect only serious ones.

6. Conclusion

For machine vision inspection for region-muras in TFT-LCD, a technique using mura levels was suggested. From the experiment performed on 200 real TFT-LCD

View publication stats

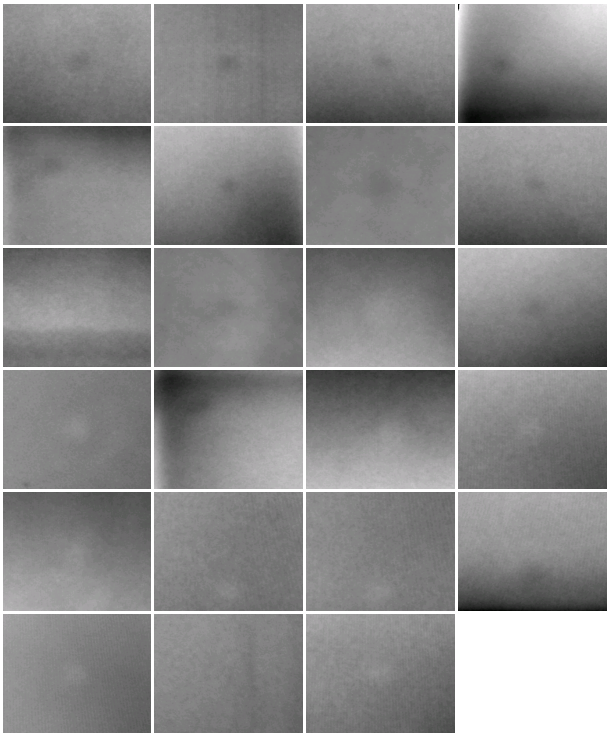

Fig. 12 Additional 23 detections not claimed by human inspection but identified to be real.

panel samples, the computed mura level was shown to corresponds to human visibility quite well. In the 200 test samples, our method was able to detect all of region-muras claimed by human inspection as well as some other region-muras not caught by human inspection. We thus expect that the identification scheme based on mura level quantification can offer manufacturers a means to control the panel quality level more consistently.

Acknowledgments

This work was supported by the Mechatronics Center of Samsung Electronics Co., Ltd. with the project of ICT 04212003-0005, and partially by the project of ICT 04212000-0008 and the BK21. The ICT at Seoul National University provided research facilities for this work.

References

[1] S. Hecht, "The visual discrimination of intensity and the Weber-Fechner law," J. Gen. Physiol., vol. 7, pp. 241, 1924.
[2] P. Moon and D.E Spencer, "The visual effect of nonuniform surrounds," J. Opt. Soc. Amer., vol. 35, pp. 233–248, 1945.
[3] H. R. Blackwell, "Contrast thresholds of the human eye," J. Opt. Soc. Amer., vol. 36, pp. 624–643, 1946.
[4] C. K. Chow and T. Kaneko, "Automatic boundary detection of the left-ventricle from cineangiograms," Comput. Biomed. Res., vol. 5, pp. 388–410, 1972.
[5] N. Otsu, "A threshold selection method from gray-level histograms," IEEE Trans. Syst., Man, Cybern., vol. SMC-9, pp. 62–66, 1979.
[6] D.A. Belsley, E. Kuh, and R.E. Welsch, Regression Diagnostics, John Wiley & Sons, USA, 1980.
[7] W. Niblack, An Introduction to Image Processing, Prentice-Hall, 1986, pp:115–116.
[8] P. J. Rousseeuw and A. M. Leroy, Robust Regression and Outlier Detection. New York: John Wiley & Sons, 1987.
[9] S. D. Yanowitz and A. M. Bruckstein, "A new method for image segmentation," Comput. Vision, Graph., Image Process., vol. 46, pp. 82–95, 1989.
[10] K. Belkacem-Boussaid, A. Beghdadi, and H. Depoisot, "Edge detection using Holladay's principle," Proc. IEEE Int. Conf. Image Processing, vol. 1, pp. 833–836, 1996.
[11] J. R. Parker, Algorithms for Image Processing and Computer Vision, John Wiley & Sons, 1997.
[12] W.K. Pratt, S. S. Sawkar and K. O'Reilly, "Automatic blemish detection in liquid crystal flat panel displays," IS&T/SPIE Symposium on Electronic Imaging: Science and Technology, 1998.
[13] Francis H. Y. Chan, F. K. Lam, and H. Zhu, "Adaptive thresholding by variational method," IEEE Trans. Image Processing, vol. 7, no. 3, pp. 468–473, 1998.
[14] Lars Heucke, Mirko Knaak, and Reinhold Orglmester, "A new image segmentation method based on human brightness perception and foveal adaptation," IEEE Signal Processing Letters, vol. 7, no. 6, pp. 129–131. June 2000.
[15] VESA Flat Panel Display Measurements Standard Ver. 2.0, June 1, 2001.
[16] R. C. Gonzalez, R. E. Woodes, Digital Image Processing. 2nd ed., Prentice Hall, 2002.
[17] Definition of measurement index (semu) for luminance mura in FPD image quality inspection, SEMI standard: SEMI D31-1102, http://www.semi.org

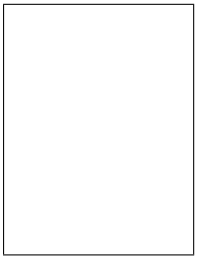

Jae Y. LEE is currently a Ph.D candidate in the School of Computer Science and Engineering at Seoul National University, Seoul, Korea. He received the BS degree (1996) in mathematics and the MS degree (1998) in computer science from the Seoul National University, Seoul, Korea. His research interests include pattern recognition and machine vision applications.

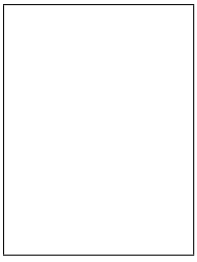

Suk I. YOO has been a professor of the School of Computer Science & Engineering at the Seoul National University, Seoul, Korea since 1985. His research interests include content-based image retrieval, machine learning, pattern recognition, and bioinformatics. He is a member of IEEE, ACM, AAAI, and SPIE. He received the BS (1977) from the Seoul National University, Seoul, Korea, the MS (1980) from the Lehigh University, Bethlehem, PA, and the Ph.D (1985) in computer engineering from the University of Michigan, Ann Arbor, MI, U.S.A..